Multimodal Excitation to Model the Quasibiennial Oscillation

P. Léard,[1,*] D. Lecoanet,[2] and M. Le Bars[1]
[1]Aix Marseille Université, CNRS, Centrale Marseille, IRPHE, Marseille 13013, France
[2]Northwestern University, Engineering Sciences and Applied Mathematics, Evanston, Illinois 60208, USA

(Received 14 February 2020; accepted 19 October 2020; published 2 December 2020)

The quasibiennial oscillation (QBO) of stratospheric winds is the most striking example of mean-flow generation and reversal by the nonlinear interactions of internal waves. Previous studies have used an idealized monochromatic forcing to investigate the QBO. Here we instead force a more realistic continuous wave spectrum. Unexpectedly, spreading the wave energy across a wide frequency range leads to more regular oscillations. We also find that different forcing spectra can yield the same QBO. Multimodal wave forcing is thus essential for understanding wave–mean-flow interactions in nature.

DOI: 10.1103/PhysRevLett.125.234501

Internal gravity waves (IGWs) are ubiquitous in geophysical and astrophysical flows, e.g., in Earth's oceans [1], atmosphere [2,3], and core [4], as well as in stellar interiors [5–7]. IGWs extract momentum from where they are excited and transport it to where they are damped [8]. In the Earth's stratosphere, these waves drive oscillations of zonal winds at equatorial latitudes, with a period of nearly 28 months. This phenomenon, known as quasibiennial oscillation (QBO) affects, e.g., hurricane activity in the Atlantic ocean [9] and the winter climate in Europe [10]. Similar reversals are observed on other planets [11,12]. The QBO is a striking example of order spontaneously emerging from a chaotic system [13], similar to magnetic field reversals in dynamo experiments [14] or mean-flow reversals in Rayleigh-Bénard convection [15].

Atmospheric waves are excited by turbulent motions in the troposphere and propagate in the stratosphere, leading to zonal wind reversals. Lindzen and Holton [16,17] proposed the QBO is due to wave–mean-flow interactions, which Plumb [18] used to construct an idealized model. The model considers the interaction of two counterpropagating gravity waves with the same frequency, wavelength, and amplitude, with a mean flow. This model was realized experimentally using an oscillating membrane at the boundary of a linearly stratified layer [19–22]. The experiments can drive oscillating mean flows similar to the QBO, as predicted by the Lindzen and Holton theory. More recently, Renaud *et al.* [23] simulated the Plumb model numerically to explain the 2016 disruption of the QBO [24,25]. Although they find regular oscillations in the mean flow at low forcing amplitudes, the mean flow becomes quasiperiodic and eventually chaotic as the forcing amplitude increases. Atmospheric forcing amplitudes are in the chaotic mean-flow regime, suggesting that the Plumb model must be refined to explain the QBO.

Because of its influence on weather events, it is crucial that the period and amplitude of the QBO are accurately modeled in global circulation models (GCMs). Because of their relatively coarse resolution, GCMs cannot compute small timescale and length scale motions like IGWs. Therefore, IGWs are parametrized in order to generate a realistic QBO. Some GCMs are able to self-consistently generate the QBO [26,27], which is considered a key test of a model's wave parametrization. The dependence of the QBO on vertical resolution and wave spectrum properties is not yet understood [28–30].

Direct numerical simulations (DNSs) have found mean-flow oscillations generated by a broad spectrum of IGWs self-consistently excited by turbulence [13]. Because DNS are expensive to run for long integration times, the influence of the forcing on the oscillations could not be studied extensively. Only a Plumb-like one-dimensional model can realistically allow for a systematic exploration.

Despite the existence of a broad spectrum of waves in nature, multiwave forcing has only been studied in [31]. Investigating three different forcing spectra, Saravanan found the QBO period is affected by the choice of the spectrum. In this Letter, we consider a wide class of wave spectra in the Plumb model, hence complementing the study of [13]. We find that forcing a broad frequency range produces regular mean-flow oscillations, even when the forcing amplitude is so large that monochromatic forcing produces a chaotic mean flow. This suggests multimodal forcing is an essential to understand wave–mean-flow interactions.

Model.—Mean-flow evolution is determined by the spatially averaged Navier-Stokes equations [32]. We define the horizontal mean flow $\bar{u}$; overbar indicates horizontal (x) average. Gravity points in the $-z$ direction, and the velocity fluctuations are (u', w'). The horizontal average evolves according to the 1D equation

$$\partial_t \bar{u} - \nu \partial_{zz} \bar{u} = -\partial_z \overline{u'w'}, \tag{1}$$

where ν is the kinematic viscosity. The mean flow is forced by the Reynolds stress term on the right-hand side of (1). In the Plumb model, the Reynolds stress comes from the self-interaction of IGWs. We excite the waves at the bottom boundary $z = 0$ and propagate the waves through a linearly stratified domain characterized by a fixed buoyancy frequency N. We nondimensionalize the problem by setting the top boundary at $z = 1$ and setting $N = 1$. Wave damping leads to vertical variation in the Reynolds stress, driving the mean flow.

We consider a superposition of waves $\psi_i = A_i(z)e^{i(k_x x-\omega_i t)}$, where ψ_i is the stream function, k_x is the horizontal wave number, and ω_i is the angular frequency. Assuming a timescale and length scale separation between the fast, short-scale IGWs and the slowly evolving, long-scale mean flow, we use the WKB approximation to derive an expression for $A_i(z)$. We also make use of the following approximations. We take the "weak" dissipation approximation, assume the background stratification is constant in space and time, and neglect wave-wave nonlinearities, except when they affect the mean flow; see details in [33] and the Supplemental Material [34]. Unlike the classical model, which uses the hydrostatic approximation [18,33], we solve the full vertical momentum equation for the wave, which allows for high-frequency IGWs. We neglect Newtonian cooling but consider diffusion of the stratifying agent (with diffusivity D), which is relevant for both laboratory experiments and the DNS described below. The inverse damping length scale is given by

$$l_i^{-1} = \frac{1}{2k_x} \times \frac{\nu + D}{(1 - k_x^2 c_i^2)^{1/2} c_i^4}, \tag{2}$$

where $c_i = [(\omega_i \mp k_x \bar{u})/k_x]$; $\mp$ accounts for the wave direction of propagation. The right-hand side of (1) is written as a sum of independent forcing terms $\sum_i \tilde{F}_i(z)$, where $\tilde{F}_i(z)$ is related to the amplitude $A_i(z)$ for each wave.

The classic Plumb model considers a single value of ω, k_x, and forcing amplitude $A(z = 0)$. To account for the multimodal excitation of waves in natural systems, we consider excitation by multiple frequencies with different forcing amplitudes. The kinetic energy of the waves is given by $E_{\text{tot}} = \int (dE/d\omega) d\omega$, and we force the waves so the energy density $dE/d\omega$ is a Gaussian in frequency centered at $\omega = \omega_0$ with a standard deviation σ. We discretize this spectrum with N_ω standing waves of frequency $\{\omega_i\}$ with frequency spacing $\omega_{i+1} - \omega_i = \Delta\omega$. The forcing amplitude is $A_i = \sqrt{2(dE/d\omega)\Delta\omega(\omega_i^2/k_x^2)}$. Our results depend only on $dE/d\omega$, not on the amplitudes of the individual modes (which vary with N_ω). We only consider a single value of $k_x = 4\pi$. This general forcing spectrum allows us to study the transition from monochromatic forcing ($\sigma \to 0$) to multimodal forcing (white noise in the limit $\sigma \to \infty$) so that we can compare our results with past monochromatic studies. We consider the dimensionless dissipation $\nu = 2.8 \times 10^{-6}$ and $D = \nu/700$, estimated from laboratory experiments [22]; we explored the ranges $\omega_0 \in [0.1; 0.45]$, $\sigma \in [10^{-4}; 3 \times 10^{-1}]$, and $E_{\text{tot}} \in [7 \times 10^{-7}; 10^{-5}]$. For comparison with previous monochromatic studies [18,23], the wave forcing Reynolds number of each individual wave goes up to $\sim$100, which is comparable to the range explored in [23]. Additional simulations were also performed with spectra representative of turbulence. Some of the results are discussed at the end of this Letter. We initialize $\bar{u}$ with a small-amplitude sinusoid. Boundary conditions for the mean flow are no-slip ($\bar{u} = 0$) at the bottom and free-slip ($\partial_z \bar{u} = 0$) at the top. The waves freely propagate out of the domain's top boundary without reflection. Section A.2 of the Supplemental Material [34] describes our spatial and temporal discretization and demonstrates numerical convergence.

We investigated the influence of top boundary conditions (BCs) on the mean-flow evolution using two-dimensional DNS of the Navier-Stokes equations [35,36]. We found the top BCs only marginally influence the period and amplitude of the oscillations and do not affect their dynamical regime [34]. We thus focus on results from our 1D model, which allows for the systematic exploration of a larger parameter space. The vertical extent of the simulation domain does not qualitatively change our results, even though some high-frequency waves have attenuation lengths greater than the domain height [34].

Results.—We investigate the influence of the forcing bandwidth on the mean-flow evolution, varying the standard deviation σ of our Gaussian excitation spectrum, but fixing the central frequency and total energy. Figure 1 shows that for narrow distributions $10^{-4} \leq \sigma < 10^{-2}$, the system produces frequency-locked oscillations, with slow oscillations in the upper part of the domain and fast oscillations in the bottom part [Fig. 1(e)]. The frequency power spectrum for $\sigma = 3 \times 10^{-4}$ [Fig. 1(h)] shows peaks at these two frequencies (f_0 and $f_0/2$), as well as at harmonic frequencies.

At $\sigma \approx 10^{-2}$, the oscillations transition from a frequency-locked regime to a quasiperiodic regime [Figs. 1(d) and 1(g)]. A second bifurcation to periodic oscillations occurs at $\sigma = 5 \times 10^{-2}$, with only one dominant frequency (plus harmonics) appearing in the corresponding spectrum [Fig. 1(f)]. Forcing spectra with wide bandwidths lead to more organized QBO-like states.

A wide bandwidth forcing spectrum includes more frequencies; naively, this would lead to chaotic mean flows. However, a wider spectrum also excites higher-frequency waves. High-frequency waves experience less damping than low-frequency waves, so they can propagate higher. Because the QBO reversal occurs at the top, we hypothesize the period and regularity of the oscillation is determined by the highest frequency wave above a threshold amplitude. At fixed wave forcing amplitude,

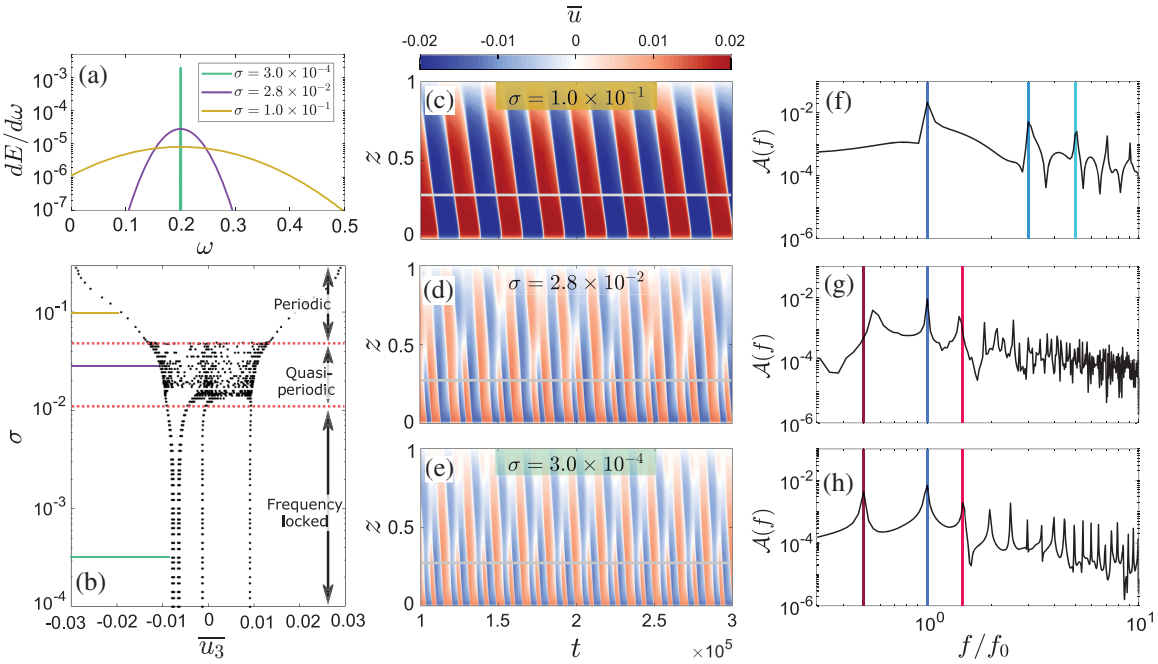

FIG. 1. Mean flows generated by a Gaussian forcing spectrum with standard deviation σ, central frequency $\omega_0 = 0.2$, and total kinetic energy $E_{\text{tot}} = 2 \times 10^{-6}$. (a) Example forcing spectra: $\sigma = 1 \times 10^{-1}$ in brown, $\sigma = 2.8 \times 10^{-2}$ in purple, and $\sigma = 3 \times 10^{-4}$ in green. (b) Poincaré map: each dot is the value of the flow $\bar{u}(z,t)$ at $z = 0.5$ (denoted $\overline{u_3}$) when $\bar{u}(z = 0.1) = 0$. Periodic oscillations are represented by two points, symmetric about $\overline{u_3} = 0$ (see Supplemental Material [34]). The asymmetry for the points below $\sigma \sim 10^{-2}$ is due to the initial condition. (c)–(e) Hovmöller diagrams of the mean flow $\bar{u}$ for different σ. (f)–(h) Amplitudes of the temporal Fourier transform taken at $z = 0.25$ for each Hovmöller diagram. Frequencies are normalized by the frequency of maximum amplitude f_0, indicated by the dark blue line. The dark red line shows $f = f_0/2$, and the other vertical lines represent harmonics.

higher-frequency waves correspond to more regular oscillations with longer periods [Fig. 2]. Furthermore, the amplitude of the mean flow is larger when forced by higher-frequency waves, because the phase velocity is larger. This means the amplitude of the mean flow is larger for the periodic oscillations forced by a wide spectrum [Fig. 1(b)].

Figure 2 shows Poincaré maps for simulations forced with different central frequencies ω_0, at fixed total energy E_{tot}. We used either a narrow distribution ($\sigma = 10^{-4}$) or a broad distribution ($\sigma = 10^{-1}$). The top panel ($\sigma = 10^{-4}$, similar to monochromatic forcing) shows a transition from periodic oscillations to nonperiodic oscillations at $\omega_0 = 0.184$. There is a second bifurcation at $\omega_0 = 0.22$ leading to periodic oscillations. The amplitude of the oscillations rises with ω_0 because the phase velocity increases. The Poincaré map for variable ω_0 (Fig. 2) is qualitatively similar to the Poincaré map for variable σ [Fig. 1(b)], suggesting that the primary effect of increasing σ is to put more power into high-frequency waves. Note, the frequency of the second bifurcation to periodic oscillations changes with domain height because the forced wave has a viscous attenuation length greater than our domain height. However, the periodic oscillations for large σ are not due to the finite domain size (see Supplemental Material [34]). The bottom panel of Fig. 2 ($\sigma = 10^{-1}$, wide spectrum) shows periodic oscillations for all ω_0. Once again, we find that a wide forcing spectrum with many frequencies will almost always generate regular periodic oscillations.

In Fig. 3, we plot Poincaré maps for different values of the total energy, with fixed ω_0 and σ. The top panel ($\sigma = 10^{-4}$, almost monochromatic forcing) qualitatively reproduces the results from [23]. As the amplitude of the monochromatic forcing increases, periodic oscillations bifurcate into frequency-locked oscillations ($E_{\text{tot}} \approx 1.4 \times 10^{-6}$), and then again into quasiperiodic or chaotic oscillations ($E_{\text{tot}} \approx 2.4 \times 10^{-6}$). On the other hand, when forcing with a wide spectrum ($\sigma = 10^{-1}$, bottom panel), we only find regular periodic oscillations.

Discussion.—Our Letter demonstrates that a broad spectrum of IGWs can generate regular mean-flow oscillations. Whereas large-amplitude monochromatic forcing often generates chaotic mean flows [23], forcing a broad spectrum of waves consistently generates periodic mean flows, similar to what is observed in the Earth's atmosphere. The mean-flow evolution appears to be determined by high-frequency waves which can propagate higher and control the mean flow's reversal. We hypothesize the disruption observed in 2016 [24,25] is due to intense

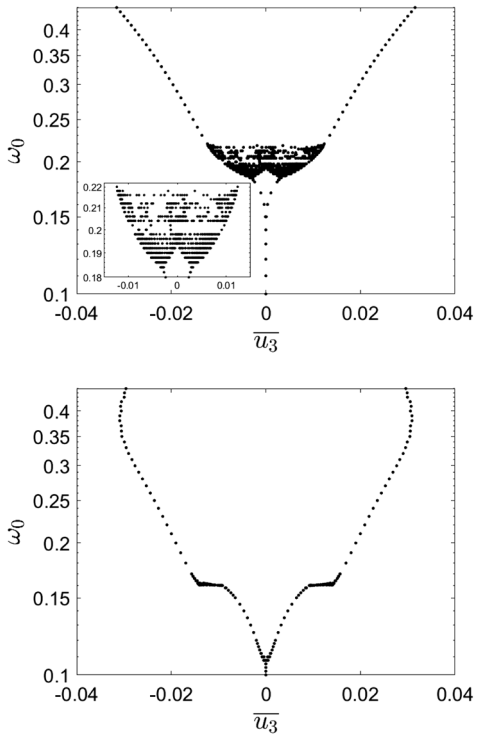

FIG. 2. Poincaré maps using the same method as Fig. 1(b) for simulations with different ω_0, with $E_{\rm tot} = 2 \times 10^{-6}$ and $\sigma = 10^{-4}$ (top) or $\sigma = 10^{-1}$ (bottom). Inset: enlargement of the frequency range $\omega_0 \in [0.18; 0.22]$ to show the transitions between periodic, frequency-locked, and quasiperiodic regimes.

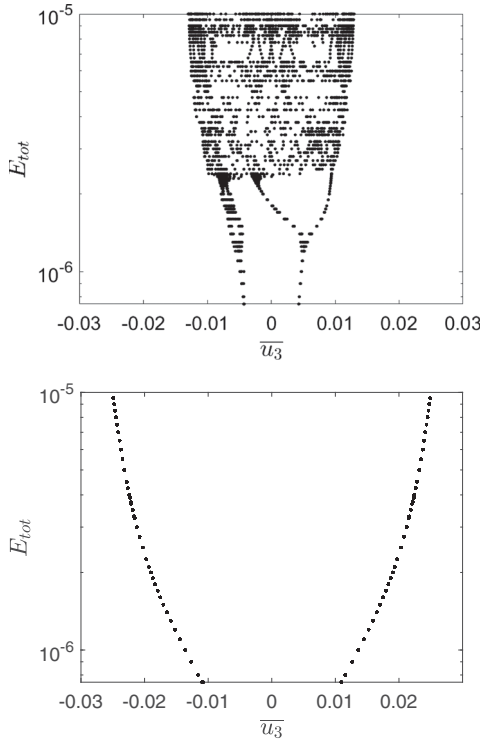

FIG. 3. Poincaré maps using the same method as Fig. 1(b) for simulations with different $E_{\rm tot}$, with $\omega_0 = 0.2$ and $\sigma = 10^{-4}$ (top) or $\sigma = 10^{-1}$ (bottom).

events that focused significant energy into waves with similar frequency and wave number. Those waves could then trigger nonperiodic reversals for a short time [23].

We have run several simulations with forcing spectra more representative of turbulence. In these simulations, we assume $dE/d\omega$ is constant for $\omega < \omega_c$ and decreases as a power law for $\omega > \omega_c$. We tested an $\omega^{-5/3}$ power law corresponding to Kolmogorov's law and an ω^{-3} power law corresponding to the energy cascade observed in rotating turbulence.

We find that different forcing spectra can lead to the same mean-flow evolution. The top panel of Fig. 4 shows a Hovmöller diagram for the $\omega^{-5/3}$ spectrum with $E_{\rm tot} = 2.5 \times 10^{-6}$. It is quantitatively similar to the Hovmöller diagram of Fig. 1(c), obtained with a Gaussian forcing and 20% less energy (oscillation periods differ by 4.5% and amplitudes by 15%). The ω^{-3} spectrum with $E_{\rm tot} = 2.8 \times 10^{-6}$ also generates a similar mean flow (bottom panel of Fig. 4; oscillation periods are equal and amplitudes differ by 14%). Since multiple wave spectra can produce the same mean-flow oscillations, reproducing the Earth's QBO in a GCM does not mean the IGW parametrization is correct.

Our simulations use parameters similar to laboratory experiments of the QBO [19,22]. In the atmosphere, wave attenuation also occurs via Newtonian cooling, which we did not include in our simulations. Besides, the forcing is stronger and viscosity is weaker. Waves deposit their

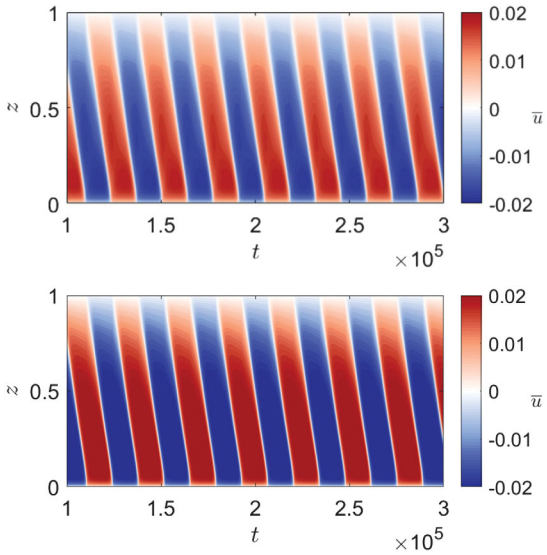

FIG. 4. Hovmöller diagram of the mean flow $\bar{u}$ in simulations with different forms of the forcing spectrum. Top: $dE/d\omega$ is constant up to $\omega_c = 0.2$ and decreases as $\omega^{-5/3}$ for higher frequencies; the total energy is $E_{\rm tot} = 2.5 \times 10^{-6}$. Bottom: $dE/d\omega$ is constant up to $\omega_c = 0.23$ and decreases as ω^{-3} for higher frequencies; the total energy is $E_{\rm tot} = 2.8 \times 10^{-6}$.

energy either via critical layers (which we include in our model) or via breaking due to wave amplification from density variations. Our calculations show the mean-flow period and amplitude is set by high-frequency waves with large viscous attenuation lengths. Although many more atmospheric waves have small viscous attenuation lengths, high-frequency waves are still more important than low-frequency waves because they do not encounter critical layers. Thus, we believe high-frequency waves likely play a key role in setting the QBO properties, just as they are important in our simulations.

In conclusion, this Letter shows that the frequency spectrum of internal gravity waves plays a key role in the generation and properties of periodic large-scale flow reversals like the QBO. Although we studied general frequency spectra, we limited our investigation to a single wave number. Future work should also include the wide range of horizontal wave numbers (10–1000 km) observed in the atmosphere, including low-frequency, planetary-scale waves which may also be an important source of momentum for the QBO [40]. Additionally, the study of the QBO in a fully coupled, convective, stably stratified model system by [13] showed that accounting for only the energy spectrum in a Plumb-like model is not sufficient to reproduce the realistic reversals; it also requires information about higher-order statistics. Clearly, reliable parametrization of this climatic metronome in GCMs still demands additional work.

The authors acknowledge funding by the European Research Council under the European Union's Horizon 2020 research and innovation program through Grant No. 681835-FLUDYCO-ERC-2015-CoG. They also thank Benjamin Favier (IRPHE, CNRS, Marseille, France) for fruitful discussions. D. L. is funded by a Lyman Spitzer, Jr. fellowship.

*Corresponding author.
leard@irphe.univ-mrs.fr

[1] C. Garrett and W. Munk, Internal waves in the ocean, Annu. Rev. Fluid Mech. **11**, 339 (1979).
[2] D. C. Fritts and M. J. Alexander, Gravity wave dynamics and effects in the middle atmosphere, Rev. Geophys. **41**, 1003 (2003).
[3] S. D. Miller, W. C. Straka, J. Yue, S. M. Smith, L. Hoffmann, M. Setvák, and P. T. Partain, Upper atmospheric gravity wave details revealed in nightglow satellite imagery, Proc. Natl. Acad. Sci. U.S.A. **112**, E6728 (2015).
[4] B. Buffett, N. Knezek, and R. Holme, Evidence for MAC waves at the top of Earth's core and implications for variations in length of day, Geophys. J. Int. **204**, 1789 (2016).
[5] C. Charbonnel and S. Talon, Mixing a stellar cocktail, Science **318**, 922 (2007).
[6] T. Straus, B. Fleck, S. M. Jefferies, G. Cauzzi, S. W. McIntosh, K. Reardon, G. Severino, and M. Steffen, The energy flux of internal gravity waves in the lower solar atmosphere, Astrophys. J. **681**, L125 (2008).
[7] T. M. Rogers, D. N. C. Lin, J. N. McElwaine, and H. H. B. Lau, Internal gravity waves in massive stars: Angular momentum transport, Astrophys. J. **772**, 21 (2013).
[8] F. P. Bretherton, Momentum transport by gravity waves, Q. J. R. Meteorol. Soc. **95**, 213 (1969).
[9] M. P. Baldwin, L. J. Gray, T. J. Dunkerton, K. Hamilton, P. H. Haynes, W. J. Randel, J. R. Holton, M. J. Alexander, I. Hirota, T. Horinouchi, D. B. A. Jones, J. S. Kinnersley, C. Marquardt, K. Sato, and M. Takahashi, The quasi-biennial oscillation, Rev. Geophys. **39**, 179 (2001).
[10] A. G. Marshall and A. A. Scaife, Impact of the QBO on surface winter climate, J. Geophys. Res. **114**, D18110 (2009).
[11] T. Fouchet, S. Guerlet, D. F. Strobel, A. A. Simon-Miller, B. Bézard, and F. M. Flasar, An equatorial oscillation in Saturn's middle atmosphere, Nature (London) **453**, 200 (2008).
[12] C. B. Leovy, A. J. Friedson, and G. S. Orton, The quasiquadrennial oscillation of Jupiter's equatorial stratosphere, Nature (London) **354**, 380 (1991).
[13] L.-A. Couston, D. Lecoanet, B. Favier, and M. Le Bars, Order out of Chaos: Slowly-Reversing Mean Flows Emerge from Turbulently-Generated Internal Waves, Phys. Rev. Lett. **120**, 244505 (2018).
[14] M. Berhanu, R. Monchaux, S. Fauve, N. Mordant, F. Pétrélis, A. Chiffaudel, F. Daviaud, B. Dubrulle, L. Mari, F. Ravelet, M. Bourgoin, P. Odier, J.-F. Pinton, and R. Volk, Magnetic field reversals in an experimental turbulent dynamo, Europhys. Lett. **77**, 59001 (2007).
[15] F. F. Araujo, S. Grossmann, and D. Lohse, Wind Reversals in Turbulent Rayleigh-Bénard Convection, Phys. Rev. Lett. **95**, 084502 (2005).
[16] R. S. Lindzen and J. R. Holton, A theory of the quasi-biennial oscillation, J. Atmos. Sci. **25**, 1095 (1968).
[17] R. S. Lindzen, An updated theory for the quasi-biennial oscillation cycle of the tropical stratosphere, J. Atmos. Sci. **29**, 1076 (1972).
[18] R. A. Plumb, The interaction of two internal waves with the mean flow: Implications for the theory of the quasi-biennial oscillation, J. Atmos. Sci. **34**, 1847 (1977).
[19] R. A. Plumb and A. D. McEwan, The instability of a forced standing wave in a viscous stratified fluid: A laboratory analogue of the quasi-biennial oscillation, J. Atmos. Sci. **35**, 1827 (1978).
[20] N. Otobe, S. Sakai, S. Yoden, and M. Shiotani, Visualization and WKB analysis of the internal gravity wave in the QBO experiment, Nagare: Jpn. Soc. Fluid Mech. **17** (1998), https://www2.nagare.or.jp/mm/98/otobe/index.htm.
[21] B. Semin, G. Facchini, F. Pétrélis, and S. Fauve, Generation of a mean flow by an internal wave, Phys. Fluids **28**, 096601 (2016).
[22] B. Semin, N. Garroum, F. Pétrélis, and S. Fauve, Nonlinear Saturation of the Large Scale Flow in a Laboratory Model of the Quasibiennial Oscillation, Phys. Rev. Lett. **121**, 134502 (2018).
[23] A. Renaud, L.-P. Nadeau, and A. Venaille, Periodicity Disruption of a Model Quasibiennial Oscillation of Equatorial Winds, Phys. Rev. Lett. **122**, 214504 (2019).

[24] S. M. Osprey, N. Butchart, J. R. Knight, A. A. Scaife, K. Hamilton, J. A. Anstey, V. Schenzinger, and C. Zhang, An unexpected disruption of the atmospheric quasi-biennial oscillation, Science **353**, 1424 (2016).
[25] P. A. Newman, L. Coy, S. Pawson, and L. R. Lait, The anomalous change in the QBO in 2015–2016, Geophys. Res. Lett. **43**, 8791 (2016).
[26] F. Lott, L. Guez, and P. Maury, A stochastic parameterization of non-orographic gravity waves: Formalism and impact on the equatorial stratosphere, Geophys. Res. Lett. **39**, L06807 (2012).
[27] F. Lott and L. Guez, A stochastic parameterization of the gravity waves due to convection and its impact on the equatorial stratosphere, J. Geophys. Res. Atmos. **118**, 8897 (2013).
[28] X.-H. Xue, H.-L. Liu, and X.-K. Dou, Parameterization of the inertial gravity waves and generation of the quasi-biennial oscillation: IGW in WACCM and generation of QBO, J. Geophys. Res **117**, D06103 (2012).
[29] J. Anstey and J. Scinocca, Simulating the QBO in an atmospheric general circulation model: Sensitivity to resolved and parameterized forcing, J. Atmos. Sci. **73**, 1649 (2016).
[30] C. Yu, X.-H. Xue, J. Wu, T. Chen, and H. Li, Sensitivity of the quasi-biennial oscillation simulated in WACCM to the phase speed spectrum and the settings in an inertial gravity wave parameterization, J. Adv. Model. Earth Syst. **9**, 389 (2017).
[31] S. Saravanan, A multiwave model of the quasi-biennial oscillation, J. Atmos. Sci. **47**, 2465 (1990).
[32] F. P. Bretherton, On the mean motion induced by internal gravity waves, J. Fluid Mech. **36**, 785 (1969).
[33] A. Renaud and A. Venaille, On the Holton-Lindzen-Plumb model for mean flow reversals in stratified fluids, arXiv: 2001.11992.
[34] See Supplemental Material at http://link.aps.org/supplemental/10.1103/PhysRevLett.125.234501 for details on the numerical model and on 2D DNS using DEDALUS, which includes Refs. [19,22,35–39].
[35] K. Burns, G. Vasil, J. Oishi, D. Lecoanet, and B. Brown, DEDALUS: Flexible framework for spectrally solving differential equations, Astrophysics Source Code Library, 2016, https://ui.adsabs.harvard.edu/abs/2016ascl.soft03015B/abstract.
[36] K. J. Burns, G. M. Vasil, J. S. Oishi, D. Lecoanet, and B. P. Brown, DEDALUS: A flexible framework for numerical simulations with spectral methods, Phys. Rev. Research **2**, 023068 (2020).
[37] R. A. Plumb, Momentum transport by the thermal tide in the stratosphere of Venus, Q. J. R. Meteorol. Soc. **101**, 763 (1975).
[38] D. Lecoanet, M. Le Bars, K. J. Burns, G. M. Vasil, B. P. Brown, E. Quataert, and J. S. Oishi, Numerical simulations of internal wave generation by convection in water, Phys. Rev. E **91**, 063016 (2015).
[39] U. M. Ascher, S. J. Ruuth, and R. J. Spiteri, Implicit-explicit Runge-Kutta methods for time-dependent partial differential equations, Applied Numerical Mathematics **25**, 151 (1997).
[40] T. J. Dunkerton, The role of gravity waves in the quasi-biennial oscillation, J. Geophys. Res. **102**, 26053 (1997).